Highly Efficient Capillary Photoelectrochemical Water Splitting Using Cellulose Nanofiber-Templated TiO_2 Photoanodes

Zhaodong Li, Chunhua Yao, Yanhao Yu, Zhiyong Cai, and Xudong Wang**

Among current endeavors to explore renewable energy technologies, photoelectrochemical (PEC) water splitting holds great promise for conversion of solar energy to chemical energy.[1–4] Light absorption, charge separation, and appropriate interfacial redox reactions are three key aspects that lead to highly efficient solar energy conversion.[5–10] Therefore, development of high-performance PEC electrodes has been concentrated largely on engineering the band structure of photoanodes, enlarging semiconductor-electrolyte interfacial area, and enabling rapid charge separation, collection, and transportation.[11,12] High porosity three dimensional (3D) nanostructures, such as branched nanowire architectures and nanofiber networks, offer extremely large surface area, excellent charge transport properties, as well as long optical paths for efficient light absorption. As a result, 3D nanostructures are the current focus of a tremendous surge of interest in PEC photoanode development.[10,13]

Among all nanostructured 3D morphologies, natural cellulose-based nanomaterials such as cellulose nanofibers (CNFs) have been attracting increasing attention in nanomanufacturing owing to their great abundance, low-cost, degradability and bio-compatibility.[14–17] CNFs are composed of elementary cellulose fibrils that are extracted directly from natural plant resources. They exhibit comparable mechanical properties (e.g., tensile strength and Young's modulus) as other broadly-used engineering materials such as carbon fibers and glass fibers.[18] CNFs also demonstrate great adsorbability in both hydrophilic and hydrophobic materials.[19] Thus, CNFs are considered as an excellent template for creating functional, fibrous 3D nanostructures that possess extremely large porosity, such as silver fiber networks,[20] nanotubular ITO sheets,[21] and porous TiO_2, ZnO and alumina nanostructures.[22–26] These CNF-templated nanostructures are very promising for the development of energy harvesting and storage devices. For example, nanostructured networks of cellulose-graphite platelet composites were applied as Li-ion battery anodes and exhibited excellent flexibility and good cycling performance.[27] Cellulose nanofiber-supported polyaniline nanocomposites showed an improved mass-specific capacitance in supercapacitor applications.[28] Cellulose fiber templates were also utilized in preparing hollow TiO_2 nanofibers as dye-sensitized solar cells (DSSCs) demonstrating significantly enhanced electron transport properties.[29] The successful application explorations of CNF-templated nanostructures suggest that the performance of PEC photoanodes might also be improved through this approach due to their similar charge transport and surface area requirements. In this paper, 3D fibrous TiO_2 nanotube architecture was synthesized by atomic layer deposition (ALD) of TiO_2 films over CNF templates. Due to the excellent hydrophilic properties of CNF films, a capillary PEC setup was developed to perform water splitting reactions outside of the electrolyte body, where electrolyte was supplied through nano/micro-channels in the CNF film driven by capillary force. Enhanced reaction kinetics and higher efficiency were observed from the capillary PEC process. In addition, modification of the calcination atmosphere can be used to engineer the chemical compounds of TiO_2 nanofibers and enable visible light photoactivity.

The CNF films were fabricated at wafer-scale via freeze-drying approach as shown in the inset of **Figure 1**a. Scanning electron microscopy (SEM) revealed a highly-porous network structure composed of dense CNFs (Figure 1a). The fibrous nanostructure was well preserved after 150 ºC ALD of TiO_2 thin film conformal coating, yielding an overall fiber diameter of ~100 nm (Figure 1b). The amorphous TiO_2 coating was then crystallized by annealing the sample at 600 ºC for 24 hours under controlled conditions (see experimental section for details). The annealing treatment crystalized the amorphous TiO_2 coating as well as burned away the CNF templates. It is noteworthy that the fibrous 3D network structure was very stable during the vigorous heat treatment and no obvious dimension or morphology change could be observed (Figure 1c), except that the core-shell fibers were converted into TiO_2 nanotubes (inset of Figure 1c).

The crystal structure of CNF-templated TiO_2 nanotubes were further investigated by transmission electron microscopy (TEM). Low-magnification TEM images clearly demonstrated the tubular TiO_2 nanostructure after annealing (Figure 1d). Thickness of the TiO_2 layer was identified to be 25–30 nm which was consistent with the 350 cycles of ALD (Figure 1e). The TiO_2 nanotubes are polycrystalline with a fairly large single-crystalline domain (~20–50 nm in one dimension). High-resolution TEM (HRTEM) revealed a single-crystalline domain region obtained from the TiO_2 nanotube. The crystal lattice spacing and the diffraction pattern from fast Fourier transform (FFT) suggest the anatase phase of the TiO_2 nanotubes. Powder X-ray diffraction (XRD) further confirmed the pure anatase TiO_2 phases after 24 hours annealing treatment (Figure S1, Supporting Information).

Z. Li, C. Yao, Y. Yu, Prof. X. D. Wang
Department of Materials Science and Engineering
University of Wisconsin-Madison
Madison, WI 53706, USA
E-mail: xudong@engr.wisc.edu
C. Yao, Dr. Z. Cai
Forest Products Laboratory
USDA Forest Service, Madison, WI 53726, USA
E-mail: zcai@fs.fed.us

DOI: 10.1002/adma.201303369

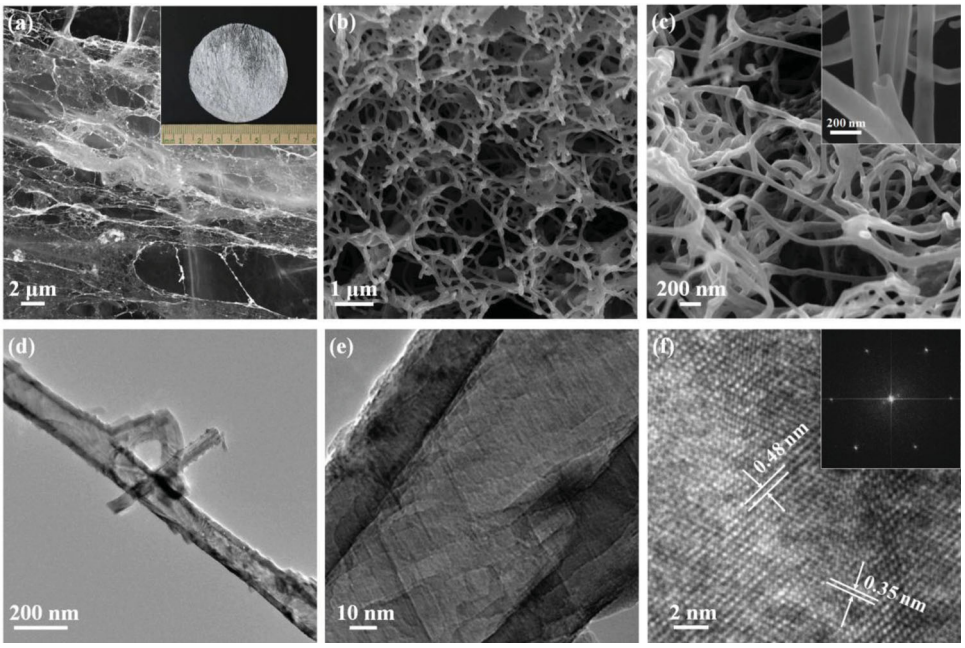

Figure 1. Morphology and structure of CNF films and templated TiO_2 nanotube structures. (a) CNF film processed on a FTO substrate; inset is a single piece of CNF film fabricated in large scale. (b) CNFs coated with TiO_2 via 350 cycles ALD at 150 °C. (c) Fibrous TiO_2 nanotube network after annealing at 600 °C for 24 hours; inset shows an enlarged broken tip revealing the hollow tubular structure. (d) TEM image of a hollow TiO_2 nanotube obtained after annealing. (e) Higher resolution TEM image showing the uniform thickness of TiO_2 walls and large crystalline domain area. (f) HRTEM image showing the single-crystal region obtained from the TiO_2 shell. The lattice spacing and FFT (inset) suggest the anatase phase.

The PEC performance of the CNF-templated TiO_2 nanotube network and the unique capability of CNF in PEC cell development were investigated using an out-of-electrolyte capillary PEC system, as schematically shown in **Figure 2**a. The active TiO_2 nanotube photoanode was placed on a conductive substrate and covered by epoxy, leaving an exposed area at the center. The photoanode bottom was in contact with a CNF film strip that was used to draw and transport electrolyte to the TiO_2 photoanode surface. The entire testing setup is shown in Figure S2. In this PEC design, the photoanode was placed outside of the electrolyte surface. Due to the excellent hydrophilic property of CNF, capillary force could drive the electrolyte to the active area quickly and continuously. Enhanced PEC reaction kinetics could be expected from the dynamic and infinitesimal electrolyte supply.

To investigate the performance of this capillary PEC design, the photocurrent density (J_{ph}) versus bias potential characteristics of both capillary PEC and conventional in-electrolyte PEC setups were measured under the same conditions. The representative *J*–*V* curves are shown in Figure 2b and c under the illumination of 100 W cm^{-2} Xe lamp source without and with AM 1.5G filter, respectively. The dark current densities

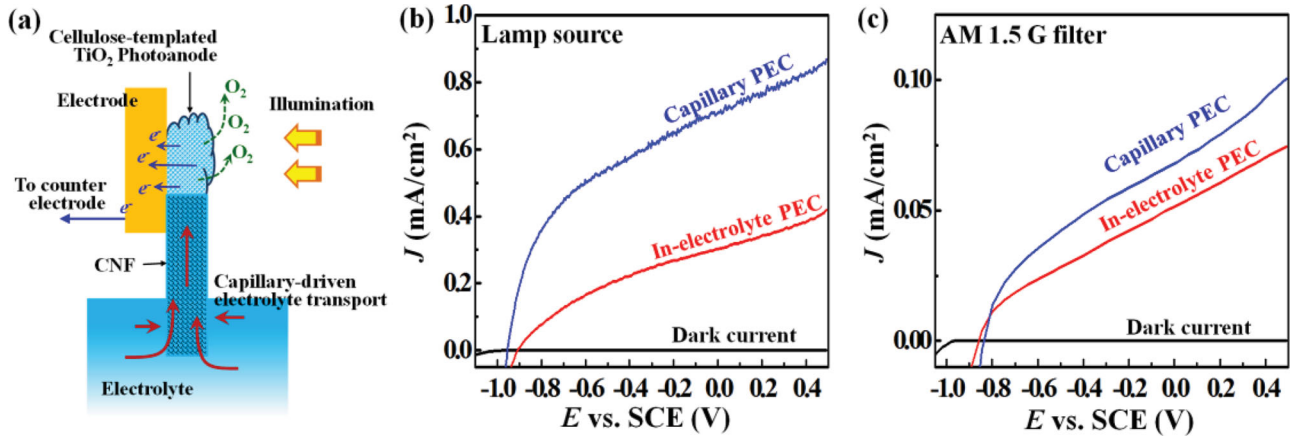

Figure 2. Capillary PEC water splitting setup and performance. (a) Schematic illustration of the capillary PEC setup. (b,c) *J*–*V* characteristics of a cellulose-templated TiO_2 photoanode measured using capillary setup and in-electrolyte setup under 100 mW cm^{-2} Xe lamp source without (b) and with (c) AM 1.5G filter.

of both setups remained at small values (<10^{-4} mA cm^{-2}) within bias potentials scanned between –1.2 V and 0.5 V (vs. SCE) demonstrating a high quality of the crystal surfaces of fibrous TiO_2 nanotubes. Generally, J_{ph} was significantly higher under Xe lamp than that under AM 1.5G filter (e.g., 0.87 vs. 0.10 mA cm^{-2}), because a large amount of UV light was cut off by the filter. This phenomenon suggests that the performance of fibrous anatase TiO_2 nanotubes photoanode was dominated by UV absorption. Under Xe lamp illumination, as shown in Figure 2b, J_{ph} measured from the capillary PEC setup ($J_{ph,ex}$, blue curve) was more than twice as much as that from the in-electrolyte setup ($J_{ph,in}$, red curve). Corresponding efficiencies were estimated using following equation:

$$\eta\% = J_{ph}(E^0_{rev} - |E_{bias} - E_{aoc}|)\frac{100}{I_0} \quad (1)$$

where E_{bias} is the bias potential; E^0_{rev} = 1.23 V is the standard state reversible potential for water-splitting reaction; and $E_{aoc} = V_{oc}$ is the open circuit voltage (vs. SCE). The capillary setup exhibited a maximum efficiency of 0.45% at ~–0.65 V; whereas the in-electrolyte setup had only a maximum efficiency of 0.16% at ~–0.45 V (Figure S3a). When AM 1.5G illumination was applied, both $J_{ph,ex}$ and $J_{ph,in}$ were significantly decreased. Although $J_{ph,ex}$ was still higher than $J_{ph,in}$, their difference became much smaller (Figure 2c). Following Equation (1), the maximum efficiencies of capillary and in-electrolyte PEC processes were found to be 0.04% at ~–0.45 V and 0.03% at ~–0.35 V, respectively (Figure S3b). Meanwhile, the saturation regions of both curves were less obvious, indicating the lower UV intensity may not generate sufficient electrons/holes to saturate the surface or defect trapping states, which facilitated the recombination of photoexcited electrons and holes.[30–32]

The stability of the cellulose-temperature TiO_2 3D fibrous photoanode and the capillary PEC configuration was further evaluated by measuring J_{ph} at a constant bias of 0.3 V (vs. SCE) under 100 mW cm^{-2} Xe lamp illumination. After an initial drop of 1.4% (J_{ph} changed from 0.73 to 0.72 mA cm^{-2}) during the first 60 minutes, J_{ph} remained at 0.72 mA cm^{-2} for 12 hours without appreciable further decrease (Figure S4). This measurement confirms good structural and functional stability of the TiO_2 photoanode. It also suggests that the capillary PEC design could function continuously and stably without any electrolyte transport or local reaction kinetic variation issues.

In order to understand performance enhancement from the capillary PEC design, a series of analyses were performed on the reaction environment and kinetics. Firstly, it is intuitive to imagine that less electrolyte body volume in front of the photoanode would result in higher light intensity that can be practically absorbed. Thus, the power densities of the illumination at fixed distances from the lamp were quantified. A linear decrease of the power density was found showing a rate of ~9.1 mW cm^{-2} per 1 cm passing length through 1 mol L^{-1} KOH electrolyte (Figure S5). Therefore, the capillary PEC design has the least amount of electrolyte covering the photoanode surface, which ensures the highest intensity of available light for absorption. This advantage becomes particularly significant when large amounts of photo-catalyst need to be applied within a confined volume of electrolyte.

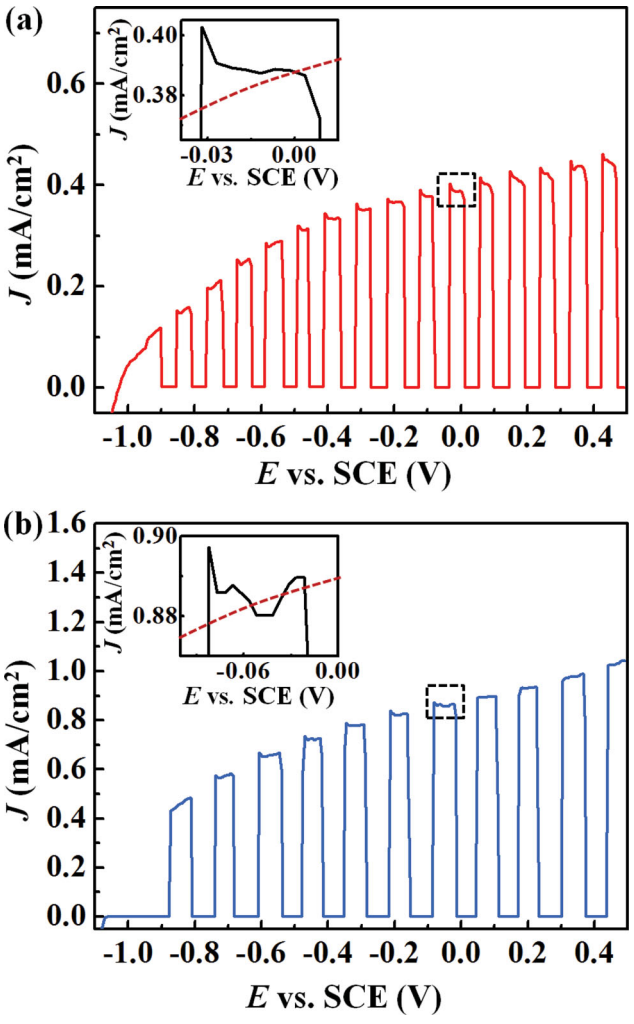

Figure 3. *J–V* characteristics of cellulose-templated TiO_2 photoanodes measured under interrupted illumination using in-electrolyte PEC setup (a) and capillary PEC setup (b). Insets are enlarged top regions of one J_{ph} cycle showing the feature of the initial current spikes.

Secondly, by performing *J–V* measurement under interrupted illumination, we found the reaction kinetics were slightly enhanced in the capillary PEC design. **Figures 3**a and b compare the *J–V* curves of the same TiO_2 fibrous photoanode collected from capillary and in-electrolyte setups under interrupted 100 mW cm^{-2} Xe lamp illumination. Both dark currents were negligibly low while the J_{ph} profiles followed a similar trace as those shown in Figure 2b. For in-electrolyte setup, the emblematical anodic current spike was obvious at the point when the illumination was on (Figure 3a and inset); whereas from the capillary PEC setup, such spikes were less distinguishable (Figure 3b and inset). These current spikes are known by evidence of accumulated photoexcited holes at the semiconductor-electrolytes interface.[33] They are a result of carrier oxidized trap states of the semiconductor,[34] or slow oxygen evolution reaction kinetics.[35,36] Such spikes can be suppressed when photoexcited holes experience less or no barrier to oxidizing the electrolyte under better interface charge transport kinetics.

Based on above discussion, the photo-oxidation reaction kinetics at TiO_2 surfaces can be compared for both PEC setups from the shape of spikes. From the area under the anodic current spike, the number of accumulated holes at the TiO_2-electrolyte interface can be estimated (Inset of Figures 3a and b), which is analogous to calculating the amount of accumulated charges in a capacitor of an RC circuit by equation:

$$I(t) = I_0 e^{-\frac{t}{\tau_0}} = \frac{dQ(t)}{dt} \quad (2)$$

where I_0 is the initial current and τ_0 is the time constant of the system. For our situation, the area density (cm^{-2}) of accumulated holes can be approximated by integrating $J(t)dt$. From both J–V curves in Figures 3a and b, the accumulated hole densities were estimated to be 8.24×10^{12} cm^{-2} for in-electrolyte PEC and 3.43×10^{12} cm^{-2} for capillary PEC. The lower interfacial hole concentration suggests a lower transient over potential ($\Delta\phi$) for oxidation reactions (see details in supplementary materials). Because identical TiO_2 fibrous photoanodes were used in both cases, $\Delta\phi$ (eV) is likely associated with the Fermi level shift of the redox couple in the electrolyte, which is directly related to the pH value in our KOH system following Equation (3).[37]

$$\Delta\varphi = 0.059 \times (pH - 14) \quad (3)$$

The pH values corresponding to the over potential found in the capillary case was calculated to be ~14.02, suggesting the OH^- concentration is slightly higher than the actual electrolyte concentration (1M KOH, pH = 14). To further confirm the pH relationship, in-electrolyte PEC was conducted using the same TiO_2 photoanode under interrupted illumination in KOH electrolytes with pH = 14.02, 14.2, respectively (Figures S6). Compared to the result shown in Figure 3a, most anodic current spikes disappeared at higher pH values. We believe higher pH value at the photoactive site was possibly due to solvent volatilization during electrolyte transport through the cellulose film. This effect is beneficial to local reaction kinetics. However, it may become impedimental in practical applications when the transportation path is too long and where the electrolyte may completely dry out. This limitation can be circumvented by encapsulating the cellulose transport path.

Another significant merit of using cellulose nanofiber as templates is its ability to modulate the chemical composition of ultimate TiO_2 nanostructures. Previous measurements were all based on fibrous anatase TiO_2 nanotubes processed by annealing in O_2 atmosphere, where the cellulose nanofibers were completely removed and the final structure appeared pure white (low right picture in **Figure 4**a). However, when annealed in vacuum (600 °C, 24 hours, 55 mTorr), the resulting TiO_2 nanostructure turned black, though the cellulose nanofiber cores were also fully removed (Figure S7). EDS analysis showed an appreciable amount of carbon (~10%) was preserved in the final TiO_2 product (Figure S8). The existence of carbon in TiO_2 and the resultant black color suggests significant visible light

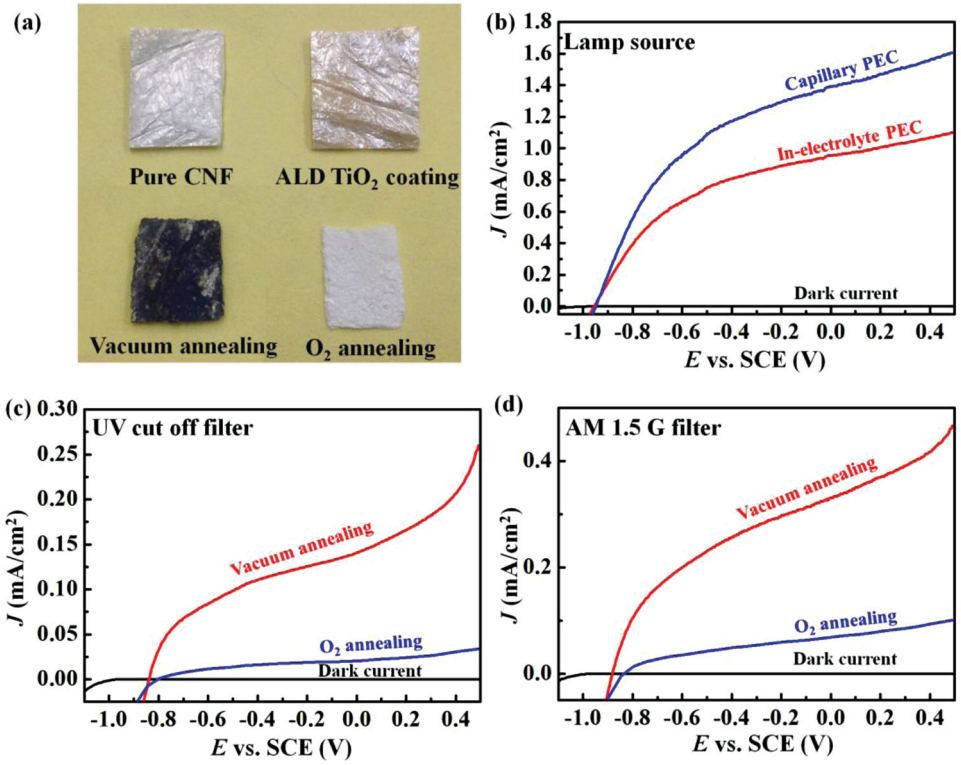

Figure 4. Effect of TiO_2 composition control. (a) Photos of CNF films before and after TiO_2 coating, and after annealing in vacuum and oxygen atmosphere. (b) J–V characteristics of "black" cellulose-templated TiO_2 photoanode measured using capillary and in-electrolyte PEC setups. (c,d) Performance comparisons of cellulose-templated TiO_2 photoanodes annealed in vacuum (red curves) and in oxygen (blue curves) measured with UV cutoff filter (c) and AM 1.5 G filter (d). All the curves were measured using capillary PEC setup.

Table 1. Summary of Photocurrent Densities and PEC Efficiencies of Fibrous TiO_2 photoanodes measured under different conditions.

PEC set up	Annealing ambient	UV cut off filter	AM 1.5 G filter	J (mA cm^{-2})	η (%)
Capillary setup	Oxygen	No	No	0.87	0.45
	Oxygen	No	Yes	0.10	0.04
	Oxygen	Yes	No	0.03	0.01
	Vacuum	No	No	1.61	0.85
	Vacuum	No	Yes	0.47	0.20
	Vacuum	Yes	No	0.26	0.09
In-electrolyte setup	Oxygen	No	No	0.42	0.16
	Oxygen	No	Yes	0.08	0.03
	Oxygen	Yes	No	0.02	0.01
	Vacuum	No	No	1.10	0.58
	Vacuum	No	Yes	0.32	0.15
	Vacuum	Yes	No	0.15	0.07

absorption and possible visible light photoactivity of the TiO_2 photoanode, which may further enhance the PEC performance. To test this hypothesis, both capillary and in-electrolyte PEC setups were applied to characterize the *J–V* curves under Xe lamp illumination. As shown in Figure 4b, both setups exhibited higher J_{ph} compared to the results from "white" TiO_2 photoanode (Figure 2b). Following Equation (1), the maximum efficiencies of the "black" TiO_2 photoanode were identified to be 0.85% and 0.58% for capillary and in-electrolyte setups, respectively.

The possible visible light photoactivity was further investigated by comparing the "black" and "white" fibrous TiO_2 photoanodes using the same capillary PEC setup and AM 1.5G and visible light (UV filter applied) illuminations, as shown in Figure 4c and d, respectively. Under both illumination conditions, J_{ph} from the "black" TiO_2 photoanode was almost an order of magnitude higher than that from the "white" TiO_2. Corresponding efficiencies were calculated (Figure S9) and summarized in **Table 1** for comparison. In general, J_{ph} and PEC efficiencies of capillary setups were higher than those obtained from in-electrolyte setup owing to less electrolyte-related light scattering and better local reaction kinetics. For both PEC setups, the vacuum annealed TiO_2 nanostructures exhibited significantly higher PEC performance compared to the ones annealed in oxygen due to the activation of visible light photoactivity. This comparison clearly shows that the capillary PEC design is able to further enhance the PEC performance in addition to those can be achieved by other strategies, such as optimizations of light absorption, surface/interface properties and charge transport. Given other key kinetic factors being well engineered, the maximum PEC efficiency could be raised to a higher level by the implementation of the capillary PEC design.

In summary, 3D CNF networks have been used as templates for fabricating PEC photoanodes via ALD of TiO_2. Annealing the cellulose-TiO_2 core-shell nanostructures created an anatase TiO_2 nanotube 3D architecture, which offered tremendous surface area for PEC water splitting. Based on the excellent hydrophilic property of cellulose, a novel capillary PEC setup has been developed. Capillary force quickly and continuously transported electrolyte to the photoanode surface during PEC water splitting. Better reaction kinetics and higher efficiency were achieved from the capillary PEC designs compared to conventional in-electrolyte PEC reactions. In addition, annealing the cellulose-TiO_2 core-shell structure in vacuum preserved the carbon elements in TiO_2, and thus activated photoactivity in the visible light region. The cellulose-based nanomanufacturing technique holds a great promise for large-area, low-cost, and green fabrication of functional nanomaterials. Using cellulose for capillary PEC design mimics the mass transport process in natural photosynthesis, where the interaction between light and reaction sites is no longer limited by the volume, surface and depth of electrolyte. Therefore, it offers a brand new solution for improving the throughput of PEC reactions.

Experimental Section

Fabrication of CNF Films: The CNFs used in our fabrication were tetramethylpiperidine-1-oxy (TEMPO) oxidized wood pulp fiber, which was prepared according to the method reported by Saito et al.[38,39] Specifically, the TEMPO-treated wood pulp fibers were mechanically homogenized on an M-110EH-30 Microfluidizer (Microfluidics, Newton, MA, USA) with a series of 200- and 87-μm chambers via two pass-throughs, then a 0.4 wt% CNF solution was obtained. After printing this CNF hydrogel on Fluorine doped Tin Oxide (FTO) glass substrates, the substrate with the hydrogel film was frozen by liquid nitrogen and ethanol bath. Next, the substrate was immediately and quickly transferred into the vacuum chamber of a Labconco 4.5 Freeze Dryer (Labconco, Kansas City, MO, USA) with stable pressure about 35 mTorr for 12 hours at room temperature, where sublimation of the ice yielded a nanofibrous structure cellulose film, 10 μm thick on the FTO.

Fabrication of TiO_2 Nanotube Photoanodes: The CNF films were loaded in ALD chamber for amorphous TiO_2 overcoating at 150 °C. The ALD growth cycle consisted of 0.5 s H_2O pulsing + 60 s N_2 purging + 0.5 s titanium tetrachloride ($TiCl_4$) pulsing + 60 s N_2 purging. 350 cycles yielded 30 nm thick amorphous TiO_2 coating. The CNF-amorphous TiO_2 core-shell structures were annealed in oxygen (600 °C, 24 hours, 390 mTorr) or vacuum (600 °C, 24 hours, 55 mTorr) to convert the amorphous TiO_2 into anatase phase. Through this process, CNFs were also removed leaving TiO_2 nanotube structures. Then, another thin film of anatase TiO_2 was coated onto the entire sample by 400-cycle ALD at 300 °C to make a continuous cover of the TiO_2 fibrous nanotubes and exposed FTO area. The last step was further annealing the samples in oxygen at 500 °C for 10 hours to eliminate carbonized cellulose residues outside of the TiO_2 crystals to avoid possible undesired electrochemical reactions during PEC measurement.

PEC Setup and Characterization: The TiO_2 nanotube networks on FTO substrate were covered by epoxy leaving an exposed active area of ~0.6 mm^2 as the photoanode. For capillary PEC setup, an additional CNF strip was adhered on the bottom side of the TiO_2 nanotube array. PEC measurements were performed in a 1 mol L^{-1} KOH (pH = 14) aqueous solution using a three-electrode electrochemical cell configuration (Figure S3). Both the conventional in-electrolyte PEC setup (immerse all active area into the KOH electrolyte) and the new capillary PEC setup (only bottom part of the cellulose strip was immersed in to KOH electrolyte) were utilized in the performance characterization of TiO_2 fibrous photoanodes. In PEC measurements, a saturated calomel electrode (SCE) was used as the reference electrode and a Pt wire was used as the counter electrode. All electrodes were connected to a potentiostat system (Metrohm Inc., Riverview, FL) for *J–V* characterization. Light illumination was provided by a 150W Xe arc lamp (Newport Corporation, Irvine, CA) and the intensity at the PEC anode position was adjusted to be 100 mW cm^{-2}. An AM 1.5G

filter and a UV cut off filter were also utilized with the lamp for PEC characterization.

Supporting Information

Supporting Information is available from the Wiley Online Library or from the author.

Acknowledgements

The authors offer thanks to Wisconsin Alumni Research Foundation (WARF) and U.S. Department of Energy, Office of Basic Energy Sciences under Award DE-SC0008711, for financial support.

Received: August 16, 2013
Published online: February 24, 2014

[1] T. Bak, J. Nowotny, M. Rekas, C. C. Sorrell, *Int. J. Hydrogen Energy* **2002**, *27*, 991.
[2] K. Maeda, K. Domen, *J. Phys. Chem. Lett.* **2010**, *1*, 2655.
[3] J. Z. Su, X. J. Feng, J. D. Sloppy, J. J. Guo, C. A. Grimes, *Nano Lett.* **2011**, *11*, 203.
[4] X. B. Chen, S. H. Shen, L. J. Guo, S. S. Mao, *Chem. Rev.* **2010**, *110*, 6503.
[5] W. J. Yin, H. W. Tang, S. H. Wei, M. M. Al-Jassim, J. Turner, Y. F. Yan, *Phys. Rev. B* **2010**, *82*, 045106(1).
[6] Y. J. Hwang, A. Boukai, P. D. Yang, *Nano Lett.* **2009**, *9*, 410.
[7] S. W. Boettcher, J. M. Spurgeon, M. C. Putnam, E. L. Warren, D. B. Turner-Evans, M. D. Kelzenberg, J. R. Maiolo, H. A. Atwater, N. S. Lewis, *Science* **2010**, *327*, 185.
[8] M. C. Hanna, A. J. Nozik, *J. Appl. Phys.* **2006**, *100*, 074510(1).
[9] J. H. Kim, T. K. Yun, J. Y. Bae, K. S. Ahn, *Jpn. J. Appl. Phys.* **2009**, *48*, 120204(1).
[10] J. Shi, Y. Hara, C. Sun, M. A. Anderson, X. Wang, *Nano Lett.* **2011**, *11*, 3413.
[11] V. K. Mahajan, M. Misra, K. S. Raja, S. K. Mohapatra, *J. Phys. D: Appl. Phys.* **2008**, *41*, 125307(1).
[12] S. Takabayashi, R. Nakamura, Y. Nakato, *J. Photochem. Photobiol. A* **2004**, *166*, 107.
[13] C. Cheng, H. J. Fan, *Nano Today* **2012**, *7*, 327.
[14] J. Zeng, R. Li, S. Liu, L. Zhang, *ACS Appl. Mater. Interfaces* **2011**, *3*, 2074.
[15] R. A. Caruso, *Angew. Chem. Int. Ed.* **2004**, *43*, 2746.
[16] S. Liu, D. Tao, H. Bai, X. Liu, *J. Appl. Polym. Sci.* **2012**, *126*, E281.
[17] R. J. Moon, A. Martini, J. Nairn, J. Simonsen, J. Youngblood, *Chem. Soc. Rev.* **2011**, *40*, 3941.
[18] B. Wang, *PhD Thesis*, University of Toronto, November, **2008**.
[19] T. Serizawa, T. Sawada, H. Okura, M. Wada, *Biomacromolecules* **2013**, *14*, 613.
[20] N. Sharifi, F. Tajabadi, N. Taghavinia, *Int. J. Hydrogen Energy* **2010**, *35*, 3258.
[21] Y. Aoki, J. Huang, T. Kunitake, *J. Mater. Chem.* **2006**, *16*, 292.
[22] Y. Shin, G. J. Exarhos, *Mater. Lett.* **2007**, *61*, 2594.
[23] C. Marichy, M. Bechelany, N. Pinna, *Adv. Mater.* **2012**, *24*, 1017.
[24] J. Huang, X. Wang, Z. L. Wang, *Nano lett.* **2006**, *6*, 2325.
[25] M. Kemell, V. Pore, M. Ritala, M. Leskelä, M. Lindén, *J. Am. Chem. Soc.* **2005**, *127*, 14178.
[26] J. T. Korhonen, P. Hiekkataipale, J. Malm, M. Karppinen, O. Ikkala, R. H. A. Ras, *ACS Nano* **2011**, *5*, 1967.
[27] L. Jabbour, C. Gerbaldi, D. Chaussy, E. Zeno, S. Bodoardo, D. Beneventi, *J. Mater. Chem.* **2010**, *20*, 7344.
[28] H. Wang, E. Zhu, J. Yang, P. Zhou, D. Sun, W. Tang, *J. Phys. Chem. C* **2012**, *116*, 13013.
[29] E. Ghadiri, N. Taghavinia, S. M. Zakeeruddin, M. Grätzel, J. Moser, *Nano Lett.* **2010**, *10*, 1632.
[30] J. Shi, X. Wang, *Energy Environ. Sci.* **2012**, *5*, 7918.
[31] S. S. Kale, H. M. Pathan, C. D. Lokhande, *J. Mater. Sci.* **2005**, *40*, 263.
[32] C. J. Liu, J. H. Wang, *Electrochemical Society, Journal* **1982**, *129*, 719.
[33] F. L. Formal, N. Tétreault, M. Cornuz, T. Moehl, M. Grätzel, K. Sivula, *Chem. Sci.* **2011**, *2*, 737.
[34] G. Horowitz, *J. Electroanal. Chem.* **1983**, *159*, 421.
[35] C. Sanchez, K. Sieber, G. Somorjai, *J. Electroanal. Chem.* **1988**, *252*, 269.
[36] M. Dareedwards, J. Goodenough, A. Hamnett, P. Trevellick, *J. Chem. Soc. Faraday Trans. 1* **1983**, *79*, 2027.
[37] A. J. Nozik, *Ann. Rev. Phys. Chem.* **1978**, *29*, 189.
[38] Y. Qing, R. Sabo, Z. Cai, Y. Wu, *Cellulose* **2013**, *20*, 303.
[39] T. Saito, M. Hirota, N. Tamura, S. Kimura, H. Fukuzumi, L. Heux, A. Isogai, *Biomacromolecules* **2009**, *10*, 1992.